Formulation for lateral resistance of lightweight thrust restraint considering elongation of geogrid

Sawada, Yutaka
Kawabata, Toshinori
Mohri, Yoshiyuki
Uchida, Kazunori

(Citation)
神戸大学都市安全研究センター研究報告,11:367-376

(Issue Date)
2007-03

(Resource Type)
departmental bulletin paper

(Version)
Version of Record

(JaLCDOI)
https://doi.org/10.24546/00518542

(URL)
https://hdl.handle.net/20.500.14094/00518542

神戸大学都市安全研究センター
研究報告，第11号，平成19年３月

FORMULATION FOR LATERAL RESISTANCE OF LIGHTWEIGHT THRUST RESTRAINT CONSIDERING ELONGATION OF GEOGRID

Yutaka Sawada[1)]

Toshinori Kawabata[2)]

Yoshiyuki Mohri[3)]

Kazunori Uchida[4)]

Abstract: In bends of pressure pipelines, thrust forces are generated due to internal pressure. Concrete blocks are installed at the bends to resist the thrust forces. However the concrete blocks will be weak points during earthquakes. In our previous study, a lightweight thrust restraint using geogrids and an anchor plate was proposed. In addition, the advantage of the proposed thrust restraint was verified by laboratory model tests and full-scale tests, and the resistance mechanism was examined by numerical analyses. Based on the failure mechanism, the maximum lateral resistance was evaluated by solving equations for the force equilibrium. In the present study, the lateral resistance of the proposed method was formulated considering the elongation of the geogrid. In addition, the calculated results were compared with the experimental results in order to verify the accuracy of the proposed formula. Furthermore parametric studies were performed to examine the influence of variations conditions on the lateral resistance. As results, it was clarified that the lateral resistance can be evaluated by the proposed formula, and the stiffness of the geogrid and the width of the anchor plate significantly influenced on the lateral resistance.

Key words: pipelines, thrust force, geosynthetics, anchor plate, lateral resistance

1. INTRODUCTION

Trust forces are generated in pipe bends depending on the bending angle, the diameter of the pipe and the magnitude of internal pressure and tend to move the bends toward the backside. Generally, concrete blocks are installed at the bends to resist the thrust forces (M.A.F.F., 1998).

On the other hand, it was reported that such a thrust block was a weak point during an earthquake due to its inertia force (Mohri et al., 1995). It can be also expected that such weighty concrete blocks induce differential settlements of pipelines on soft ground. For these problems, as shown in Fig.1, a new lightweight thrust restraint using geogrids and an anchor plate was

proposed by Kawabata et al. (2004). In our previous study, the effectiveness was verified by laboratory model tests using the model pipe having a diameter of 90 mm (Kawabata et al., 2004). As the results, the lateral resistance of the proposed restraint was approximately 1.6 times of that of the model pipe without the restraint.

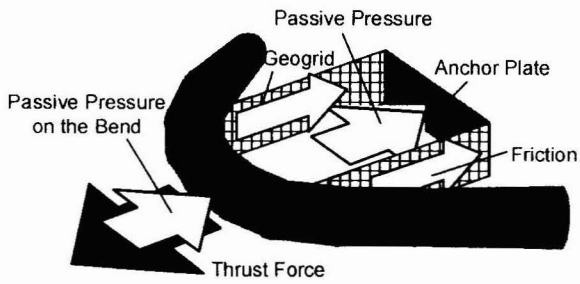

Fig.1 Schematic diagram of lightweight thrust restraint

In addition, the resistance mechanism of the proposed method was examined by image analyses for ground surface in model tests (Sawada et al., 2006a) and numerical analyses (Kawabata et al., 2006a). As the results, two failure mechanisms were observed, and they depended on the depth of cover and the length of the geogrid. Sawada et al. (2006a) assumed the failure surfaces of the ground in front of the anchor plate based on the failure mechanisms and evaluated the maximum lateral resistance of the proposed restraint by solving equations for the force equilibrium. Sawada et al. (2006b) also formulated the relationships between the lateral displacement and the lateral resistance using a parabolic function on the assumption that geogrids were entirely rigid.

Further large scale tests were carried out using a bend (ϕ300) and two type geogrids by Kawabata et al. (2006b). As results, it was found that the lateral resistance was strongly influenced by the elongation of the geogrid. Thus, it is important to evaluate the lateral resistance considering the elongation of the geogrid.

Recently geogrids are widely used to improve the stability of embankments. Many researchers focused on the soil-geogrid interaction by pull-out tests (e.g. Palmeria and Milligan, 1989) or direct shear tests (e.g. Nakamura *et al*, 1999) putting geogrid under the various experimental conditions.

Theoretical formulations for the relationship between the pull-out resistance and the pull-out displacement were suggested by many researchers (e.g. Mitachi et al., 1991). Imaizumi et al. (1995) suggested a simple elastic formula considering the deformation of geomembranes and verified the accuracy of the formula from comparison with experimental results.

In the present study, the lateral resistance by proposed method was evaluated considering the elongation of the geogrid. The formulation was carried out in two steps. Firstly, the pull-out resistance of the geogrid was formulated based on the concept proposed by Imaizumi et al. (1995). Secondly the passive resistance acting on the anchor plate was formulated. In addition, the accuracy of the formula was verified by comparing with experimental results. Furthermore, in order to examine the influence of various conditions on the lateral resistance, parametric studies were performed.

2. FORMULATION FOR LATERAL RESISTANCE BY LIGHTWEGHT THRUST RESTRAINT

The lateral resistance provided by the lightweight thrust restraint is divided into two resistant components, one is the pull-out resistance of the geogrid and the other is passive resistance acting on the anchor plate, as shown in Fig.1. The relationships between the lateral resistance and the displacement of the bend can be postulated as shown in Fig.2. (i) Firstly the pull-out resistance increases with the displacement of the bend up to the displacement Y'. In this step, geogrids are gradually pulled out from the forefront to the posterior end of the geogrid. (ii) Secondly, after the end of the geogrid is pulled out, passive resistance acting on the

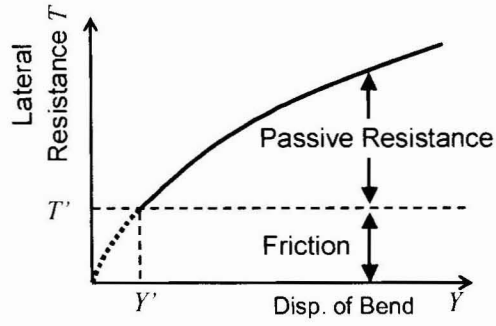

Fig.2 Schematic diagram of relationships between displacement of bend and lateral resistance

anchor plate develops. The pull-out resistance is formulated based on the elastic equation proposed by Imaizumi et al (1995). Imaizumi et al. focused on the geomembrane placed horizontally in the ground. It should be note that the geogrids are placed vertically in proposed method as shown in Fig.1.

Fig.3 schematically shows the frictional stress along geogrid and the elongation of the geogrid. Considering the elongation $ds(x)$ in the element geogrid having a length of dx, tensile strain $\varepsilon(x)$ is expressed as follow,

$$\varepsilon(x) = \frac{ds(x)}{dx} = \frac{t(x)}{E} \quad (1)$$

in which $t(x)$ is the tensile force per unit width (kN/m), E the is tensile stiffness of the geogrid per unit width (kN/m).

In case of placing the geogrid vertically, the geogrid is subjected to horizontal earth pressure. Frictional stress τ can be obtained by assuming the earth pressure distribution as a trapezium form.

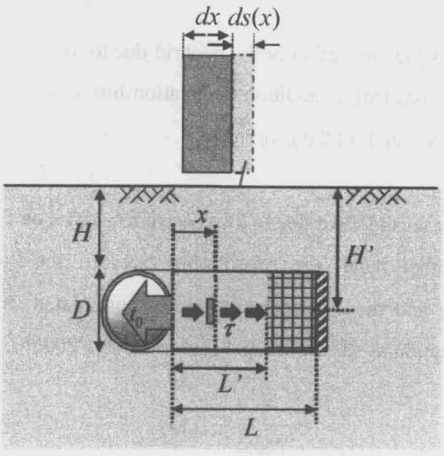

Fig.3 Schematic diagram of frictional stress along geogrid and elongation of geogrid

$$\tau = K_0 \cdot \gamma_t \cdot H' \cdot \tan\delta \quad (2)$$

Here K_0 is Jaky's coefficient of earth pressure at rest, γ_t is the unit weight of soil (kN / m^3), H' is the depth from the ground surface to the center of the geogrid (m), δ is the friction angle between soils and geogrids (°). From the force equilibrium, the pull-out resistance can be expressed as follows,

$$t_0 = t(x) + 2 \cdot \tau \cdot x \quad (3)$$

where t_0 is the pull-out resistance per unit width (kN/m). Substituting Eqs (2) and (3) into Eq.(1), $ds(x)$ can be expressed as follows.

$$ds(x) = \frac{t_0 - 2 \cdot K_0 \cdot \gamma_t \cdot H' \cdot \tan\delta \cdot x}{E} dx \quad (4)$$

Considering that τ develops up to L', the pull-out displacement Y can be obtained by integrating Eq.(4) from 0 to L'.

$$Y = \int_0^{L'} ds(x) = \frac{t_0 \cdot L' - K_0 \cdot \gamma_t \cdot H' \cdot \tan\delta \cdot L'^2}{E} \quad (5)$$

Solving Eq.(3) under the boundary condition ($x = L' : t'(L') = 0$), the following Eq.(6) can be obtained.

$$L' = \frac{t_0}{2 \cdot K_0 \cdot \gamma_t \cdot H' \cdot \tan\delta} \quad (6)$$

The pull-out resistance t_0 can be obtained by substituting Eq.(5) into Eq.(6). Thus, for both side geogrids, the total pull-out resistance can be expressed as follow,

$$T = 4 \cdot D \cdot \sqrt{Y \cdot K_0 \cdot \gamma_t \cdot H' \cdot \tan\delta \cdot E} \quad (7)$$

where T is the total pull-out resistance (kN) and D is the diameter of the bend or the height of the geogrid (m). This equation can be applied from 0 to the displacement Y'. Y' can be obtained by integrating Eq.(4) from 0 to L.

$$Y' = \frac{K_0 \cdot \gamma_t \cdot H' \cdot \tan\delta \cdot L^2}{E} \quad (8)$$

Here L is the length of the geogrid (m). At the displacement Y', the pull-out resistance T' can be obtained by substituting Eq.(8) into Eq.(7).

$$T' = 4 \cdot D \cdot K_0 \cdot \gamma_t \cdot H' \cdot \tan\delta \cdot L \quad (9)$$

In case of $Y \geq Y'$, the anchor plate contributes to the increase of the lateral resistance. Considering the elongation of the geogrid due to the passive resistance on the anchor plate, the displacement of the bend can be expressed as the following equation.

$$Y - Y' = Y_G + Y_A \quad (10)$$

Note that Y_G is the elongation of the geogrid due to the passive resistance on the anchor plate (m) and Y_A is the displacement of the anchor plate (m). In addition the relationship between the tensile stress and the tensile strain is obeying Hooke's low up to the rupture strength of the geogrid.

$$T_G = E \cdot D \cdot Y_G / L \quad (11)$$

Here T_G is the tensile force due to the passive resistance on the anchor plate (kN).

On the other hand, the relationship between the passive resistance T_A and the displacement Y_A was formulated using a parabolic function as shown in Fig.4 (Sawada et al., 2006b).

$$T_A = a \cdot \sqrt{Y_A}$$
$$a = \frac{T_{A\max}}{\sqrt{Y_{A\max}}} \quad (12)$$

Note that T_{Amax} is the maximum passive resistance and Y_{Amax} is the displacement of the anchor plate at T_{Amax}. In previous study, T_{Amax} was evaluated by solving equations of the force equilibrium for the failure mechanisms as shown in Fig.5. (Sawada et al., 2006a) For $H/L \leq 0.6$,

$$T_{A\max} = W \cdot \tan\phi' + \left(\frac{L}{3} \cdot A_1 + \frac{B}{2} \cdot A_2\right) \cdot \gamma_t \cdot H^2 \quad (13)$$

where

$$W = L \cdot B \cdot \gamma_t \cdot (H + D) + \frac{L^2 \cdot \tan\alpha \cdot H \cdot \gamma_t}{3}$$
$$A_1 = \frac{2}{\cos\beta}\left(K_0 \cdot \cos^2\beta + \sin^2\beta\right) \cdot (1 - \sin\beta)\tan\phi'$$
$$+ \frac{1}{\cos\alpha} K_0 \cdot \left(\cos\alpha \cdot \tan\phi' - \sin\alpha\right) + \tan\alpha \cdot K_a$$
$$A_2 = K_p - K_a$$

and for $H/L > 0.6$,

$$T_{A\max} = b \cdot L \cdot B \cdot \gamma_t \cdot (2 \cdot H + D)\tan\phi' \quad (14)$$

Here H is the depth of cover (m), ϕ' is the effective internal friction angle (°), B is the width of the anchor plate (m), K_a is Rankin active earth pressure coefficient, K_p is Rankin passive coefficient and b (= 1.3) is a coefficient for the increase of normal earth pressure acting on the shear plane. In addition, α and β ($\alpha = \phi'/2$, $\tan\beta = L\tan\alpha / H$) are the angle of the failure mass as shown in Fig.5. In addition, Y_{Amax} can be given as,

$$Y_{A\max} = d_{peak} \cdot L \quad (15)$$

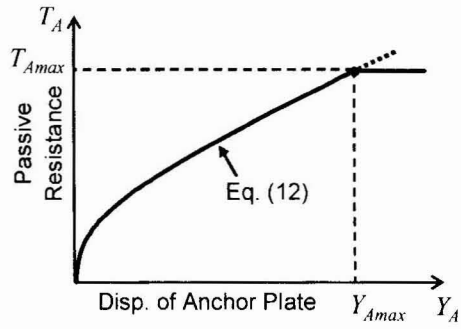

Fig.4 Schematic diagram of relationships between displacement of anchor plate and passive resistance

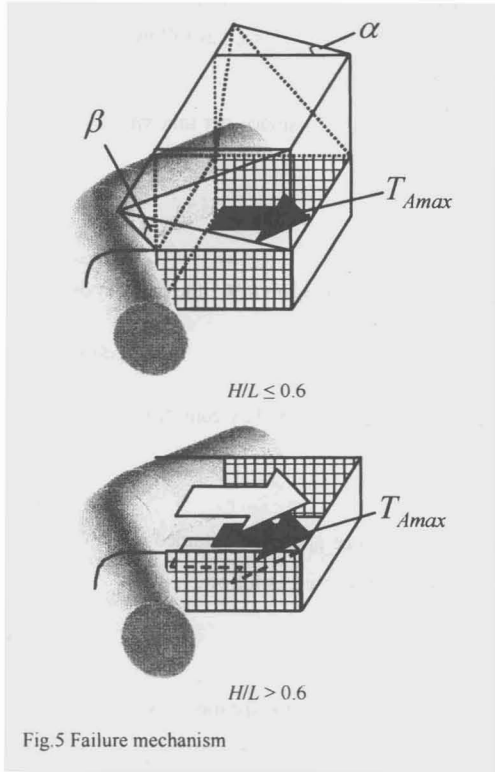

Fig.5 Failure mechanism

in which d is the shear displacement ratio at the maximum shear stress in a direct shear test. Note that the displacement ration is defined as the ratio of the shear displacement to the diameter of the specimen in direct shear test.

Considering the force equilibrium, the relation between T_G and T_A can be expressed as follow.

$$T_A = 2 \cdot T_G \quad (16)$$

The passive resistance T_A can be obtained by solving simultaneous equations of Eqs (10), (11), (12) and (16). Consequently the total lateral resistance T can be obtained considering the frictional resistance T' given by Eq.(9).

$$T = T'+T_A$$
$$= T'+a\cdot\left(\frac{-\varphi+\sqrt{\varphi^2+16\cdot(Y-Y')}}{4}\right) \quad (17)$$

where

$$\varphi=\frac{a\cdot L}{E\cdot D}.$$

3. LARGE SCALE TESTS

3.1 Outline of Tests

Fig.6 shows a cross section of a test pit having a width of 5.4 m, a length of 8.4 m and a height of 4.0 m. In the pit, a foundation bed having a thickness of 1 m was laid and a bend having an angle of 90 degrees and straight pipes having a diameter of 0.3 m were installed on the foundation. After installing the pipeline, geogrids and an anchor plate were connected with the bend and they were backfilled up to 0.6 m. Two types of geogrids were used in these tests and the results of tensile tests are shown in Fig.7. Stiffness of Geogrid A is larger than Geogrid B as shown Fig.7. A rigid steel plate having a dimension 1.2 m × 0.3 m was used as the anchor plate. The ground was compacted with a vibration compactor every 0.15 m. After backfilling, the internal water pressure was loaded by a hydrostatic pump. In these tests, the displacement of the bend and the tensile strain in geogrid were measured with pulley type displacement transducers and strain gauges respectively as shown in Fig.6. Table 1 summarized the test conditions for three cases. Three cases are different in the length and the tensile stiffness of the geogrid.

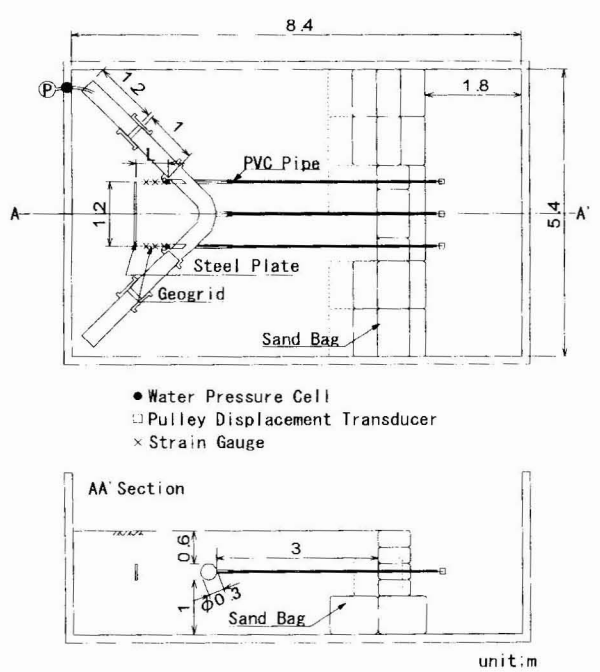

Fig.6 Cross section of test

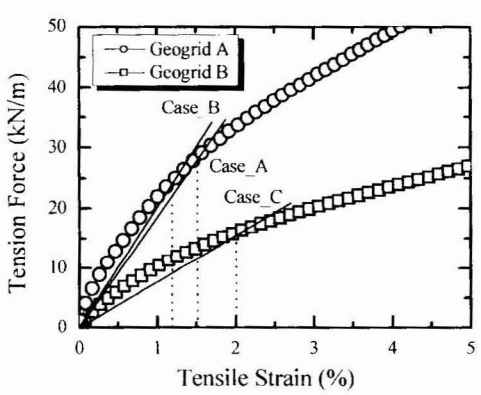

Fig.7 Relationships between tensile strain and tensile force

Table 1 Summary of test cases

	Type of Geogrid	L
Case_A	Geogrid A	0.50
Case_B	Geogrid A	0.83
Case_C	Geogrid B	0.50

Note: L is length of Geogrid (m).

3.2 Test Results and Discussions

Fig.8 shows relationships between the displacement of the bend and the lateral resistance of the proposed method. Note that the lateral resistance can be obtained by multiplying the tensile strain in forefront of the geogrid by the tensile stiffness. From Fig.8 the lateral resistance in Case_A and Case_B using high stiffness geogrids is much larger than that in Case_C. The difference is about 1.8 times. Thus the lateral resistance is extremely influenced by the stiffness of the geogrid. Comparing Case_A with Case_B, the difference can not be clearly seen. The detail of this behavior is explained in parametric studies.

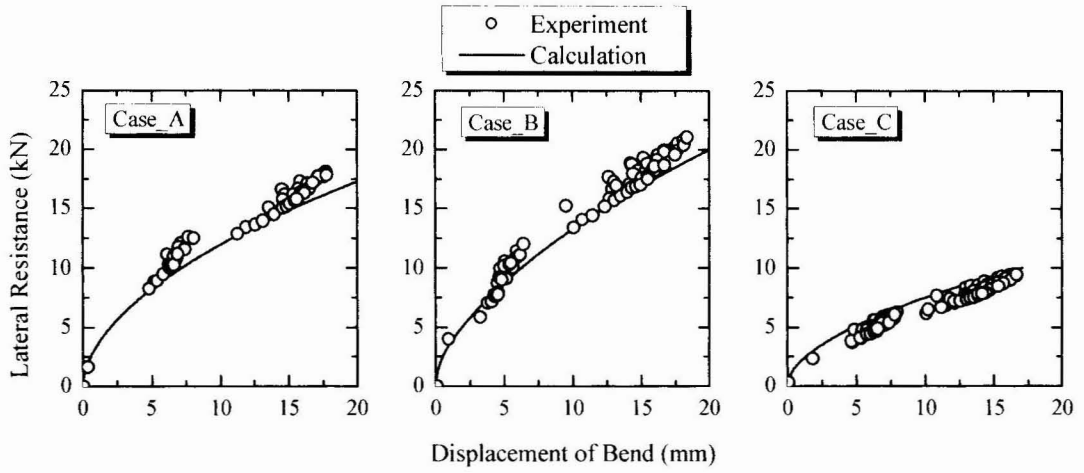

Fig.8 Relationships between displacement and lateral resistance

4. COMPARISON OF RESULTS FROM TESTS AND ESTIMATIONS

Table 2 summarized parameters used in the proposed formula. The unit weight of soils γ_t was given as the average dry density measured in tests. In order to determine the internal friction angle ϕ' and the shear displacement ratio d, direct shear tests were conducted. The direct shear tests were conducted under normal pressure which is equivalent to the depth of the embedment in large scale tests. In addition, the dry density of the specimen was approximated as 17.0 kN / m^3 for Case_A and Case_B and 16.5 kN /m^3 for Case-C. The relationships between the normal stress and the maximum shear stress are shown in Fig.9. From Fig.9, the internal friction angle is 38.8° and 32.2° for 17.0 kN / m^3 and 16.5 kN / m^3 respectively. In addition, Fig.10 shows the relationships between the displacement ratio and the shear stress. From Fig.10, d is 3.60×10^{-2} and 4.70×10^{-2} for 17.0 kN / m^3 and 16.5 kN / m^3 respectively. According to P.W.R.C. (2000), the friction angle, δ, between soils and geogrids can be assumed as equal to the internal friction angle. Thus, δ is 38.8° and 32.2° for the ground of 17.0 kN / m^3 and 16.5 kN / m^3 respectively. The tensile stiffness of the geogrid, E, was determined based on results of the tensile tests of the geogrid as shown in Fig.7. Namely the strain values at the displacement of the bend of 15 mm are 1.5 % for Case_A, 1.2 % for Case_B and 2.0 % for Case_C. In practical design, it is reasonable to give E a secant at 2 %.

Comparisons of the lateral resistance from large scale tests and calculations are shown in Fig.8. The lateral resistances were calculated from Eq.(7) or Eq.(17). Note that calculated results are indicated with lines. From Fig.8, it can be seen that calculated results give good agreement with experimental results although they are slightly underestimated in Case_A and Case_B and overestimated in Case_C. From this result, it can be judge that the lateral resistance can be predicted by the proposed formula considering the elongation of the geogrid.

Table.2 Summary of parameters in analysis

	D	H	L	B	γ_t	$\phi'(\delta)$	d	E
Case_A	0.3	0.60	0.50	1.20	16.8	38.2	3.60×10^{-2}	1875.0
Case_B	0.3	0.60	0.83	1.20	17.0	38.2	3.60×10^{-2}	2250.0
Case_C	0.3	0.60	0.50	1.20	16.4	32.2	4.70×10^{-2}	790.0

Note: D is pipe diameter (m), H is depth of cover (m), L is length of side restraint (m), B is width of anchor plate (m), γ_t is unit weight of soil (kN/m^3), ϕ' is effective internal friction angle (°), δ is friction angle between soils and geogrid (°), d is shear displacement ratio at maximum shear stress (%), E is tensile stiffness of geogrid (kN / m).

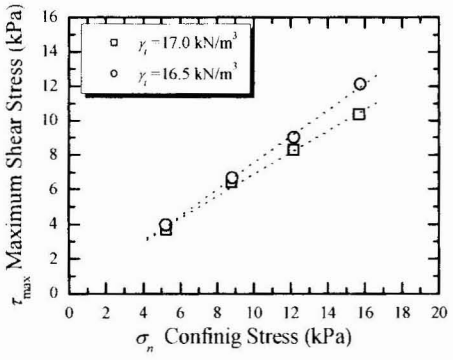

Fig.9 Relationships between tensile strain and tensile force

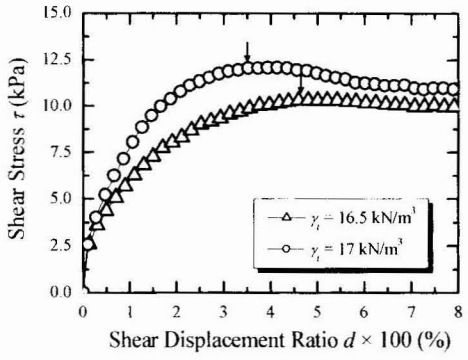

Fig.10 Relationships between shear displacement ratio and shear stress

5. INFLUENCE OF VARIOUS CONDITIONS ON LATERAL RESIATNECE

A limited number of investigations were carried out in large-scale tests in preceding session. It is apparent that Eq.(17) is a function of the stiffness, the length, the width, the height of the geogrid and so on. It is important to examine the behavior of the proposed thrust restraint under various conditions. However, a number of experimental investigations are not only expensive and but also time-consuming. In the present study, parametric studies have been carried out in order to investigate the influence of the various conditions on the lateral resistance of the proposed method. In the parametric studies, parameters were varied based on Case_A as shown in Table 2. Here it should be noted that the errors between experiments and calculations remain not to be removed.

5.1 Influence of Stiffness of Geogrids

Fig.11 shows the relationships between the displacement of the bend and the lateral resistance for various stiffness of the geogrid. From these results, it can be seen that the lateral resistance tends to increase with the tensile stiffness. Comparing the secant slope at displacement of 20 mm in case of E = 3000 kN / m and E = 500 kN / m, the former (0.92 kN / mm) is 1.6 times as large as the later (0.56 kN / mm). In addition, considering $E = \infty$, lateral resistance can be calculated from Eq.(17) as follows.

$$\lim_{E \to \infty} T = T' + a\sqrt{Y} \qquad (18)$$

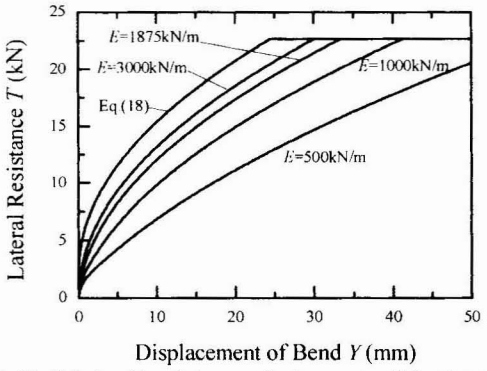

Fig.11 Relationships between displacement of bend and lateral resistance (E is from 500 to 3000 kN/m^2)

In Eq.(18), the first term expresses the frictional resistance and the second term expresses the passive resistance associated with the displacement of the anchor plate as shown in Eq.(12). The calculated result from Eq.(18) is also indicated in Fig.11. It can be understood that this curve is an upper limit of the lateral resistance under the present condition.

On the other hand, the peak value of the lateral resistance is a constant value regardless of the stiffness of the geogrid. This reason is that the failure mechanism shown in Fig.5 is not influenced on the stiffness of the geogrid.

5.2 Influence of Length of Geogrids

Fig.12 shows the relationships between the displacement of the bend and the lateral resistance for various length of the geogrid. It is found that the peak value of the lateral resistance tends to increase with the length of the geogrid. This is due to the increase of the volume of the soil mass in front of the anchor plate as shown in Fig.5. However, at initial displacement of the bend up to 10 mm, the difference in each case is found to be slight. For this reason, it can be considered that long geogrids are easy to deform. In addition, due to this reason, it can be considered that the difference between in Case_A and Case_B was slight in Fig.8.

In practical design, the increment of the lateral resistance at initial displacement of the bend is significantly important. Therefore, it can be judged that the influence of the length of the geogrid on the lateral resistance is small.

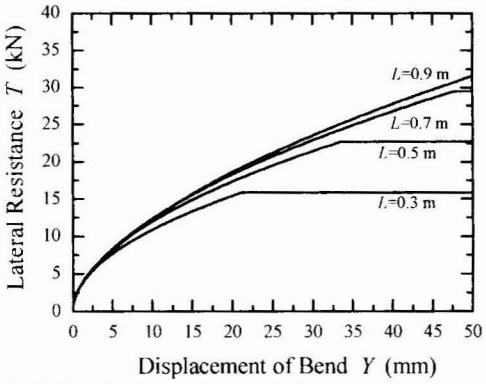

Fig.12 Relationships between displacement of bend and lateral resistance (L is from 0.3 to 0.9 m)

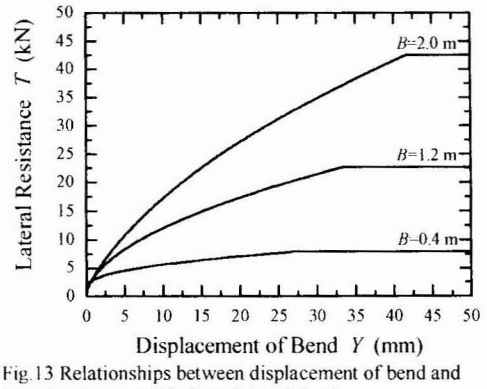

Fig.13 Relationships between displacement of bend and lateral resistance (B is from 0.4 to 2.0 m)

5.3 Influence of Width of Anchor Plate

Displacement-resistance curves for change of the width of the anchor plate are indicated in Fig.13. As be expected, it is apparent that the lateral resistance tends to increase with the width of the anchor plate. The resistance for B = 2.0 m is about 3 times as large as that for B = 0.4 m at the displacement of 10 mm. In addition, it can be seen that the peak value of the lateral resistance also increases with the increase of the width of the anchor plate. Judging from these results, the effect of the anchor width is significantly large.

5.4 Influence of Internal Friction Angle of Soils

Fig.14 shows the relationships between the displacement of the bend and the lateral resistance for variation of the internal friction angle of soils. In general, the friction angle between soils and geogrids also increases with the internal friction angle. In Fig.14, δ is also changed with ϕ'. From Fig.14, as might be expected, the maximum resistance increases with the increase of ϕ'. The resistance for ϕ' = 45° is about 1.6 times as large as that for ϕ' = 25° at the displacement of 10 mm. It can be judged that the effect of the strength of the backfill materials is significantly large.

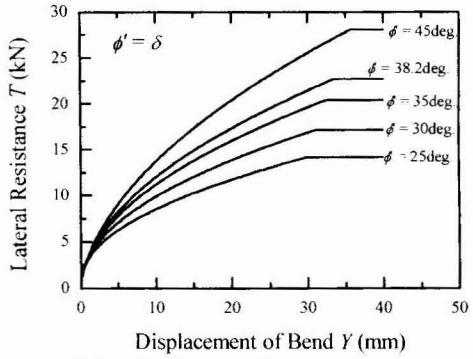

Fig.14 Relationships between displacement of bend and lateral resistance (ϕ' is from 25 to 45 deg.)

6. CONCLUSIONS

In this study, for the lightweight thrust restraint with geogrids and an anchor plate, the lateral resistance was formulated considering the elongation of the geogrid in order to establish the detail design. In addition, calculated resistances were compared with results in large scale experiments to examine the accuracy. As the results, a good agreement can be seen between calculated results and experimental results. It can be judged that the lateral resistance of the proposed thrust restraint can be predicted by the proposed formula. Furthermore, to examine the influence of various conditions on the lateral resistance, parametric studies were perfumed. Consequently it was found that the lateral resistance strongly depended on the stiffness of the geogrid, the width of the anchor plate and the frictional angle of the backfill materials. In addition, it was found that the influence of the length of the geogrid was not considerably important factor for the initial lateral resistance.

REFFERENCE

1) M.A.F.F., *Ministry of Agriculture, Forestry and Fisheries, Design Standard for Pipeline*, 1998.

2) Mohri, Y., Yasunaka, M. and Tani, S., Damage to Buried Pipeline Due to Liquefaction Induced Performance at the Ground by the Hokkaido-Nansei-Oki Earthquake in 1993, *Proceedings of First International Conference on earthquake Geotechnical Engineering*, IS-Tokyo, pp.31-36, 1995.

3) Kawabata, T., Uchida, K., Ling, H. I., Nakase, H., Sawada, Y., Hirai, T. and Saito, K., Lateral Loading Tests for Buried Pipe with Geosynthetics, *Proceedings of Geo-Trans 2004*, ASCE, Vol.1, pp.609-616, 2004.

4) Kawabata, T., Sawada, Y., Uchida, K., Kitano, T., Ling, H. I., Hirai, T. and Saito, K., Model tests for new lightweight thrust restrain using geogrid, *Geosynthetics*, Edited Kuwano, J. and Koseki, J., pp.1695-1698, Millpress, Rotterdam, 2006a.

5) Sawada, Y., Kawabata, T., Takami, M., Watanabe, K., Mohri, Y. and Uchida, K., Estimation for Incremental Lateral Resistance by Lightweight Thrust Restraint Using Geosynthetics, *Proceedings of the 41st Japan National Conference on Soil Mechanics and Foundation Engineering*, JGS, pp.1789-1790, 2006a.

6) Sawada, Y., Kawabata, T., Mohri, Y. and Uchida, K., Estimation Method for Incremental Resistance on Lightweight Thrust Restraint Using Geogrid, *Geosynthetics Engineering Journal*, JCIGS, Vol.21, pp.97-104, 2006b.

7) Kawabata, T., Sawada, Y., Ogushi, K., Totsugi, A., Hironaka, J. and Uchida, K., Large-Scale Experiments on Pipe Bend with Lightweight Thrust Restraint Using Geogrid, *Geosynthetics Engineering Journal*, JCIGS, Vol.21, pp.105-110, 2006b.

8) Palmeria, E.M. and Milligan, G.W.E., Scale And Other Factors Affecting the Results of Pull-Out Tests of Grids Buried Sand, *Geotechnique*, London, Vol.39, No.3, pp.511-524, 1989.

9) Nakamura, T., Mitachi, T. and Ikeura, I., Direct Shear Testing Method as a Means for Estimating Geogrid-Sand Interface Shear-Displacement Behavior, *Soils and Foundations*, JGS, Vol.39, No.4, pp.1-8, 1999.

10) Mitachi,T., Yamamoto,Y and Muraki,S., Evaluation of Pull-out Performance of Geogrid Taking Account of the Material Stiffness, *Geosynthetics Engineering Journal*, JCIGS, Vol. 6, pp.93-99, 1991.

11) Imaizumi, S., Takahashi, S., Yokoyama, Y. and Nishigata, T., Evaluation of Pull-Out Behavior of HDPE Geomembrane Embedded in Sand, *Journal of Geotechnical and Geoenvironmental Engineering Division*, JSCE, (No. 511/III-30), pp.155-162, 1995.

12) P.W.R.C., Design and Construction Manual for Soil Structures Reinforced with Geotextiles, Second Edition, Public Works Research Center, Tokyo, pp.54-59, 2000.

Author: 1) Yutaka SAWADA, Doctoral Student, Graduate School of Science and Technology, Kobe University, 2) Toshinori KAWABATA, Associate Professor, Graduate School of Agricultural Science, Kobe University 3) Yoshiyuki MOHRI, Ph.D., Research Manager, National Institute of Rural Engineering 4) Kazunori UCHDA, Professor, Graduate School of Agricultural Science, Kobe University